
CityNav: Language-Goal Aerial Navigation Dataset with Geographic Information

Jungdae Lee^{1*}, Taiki Miyanishi^{2,4,5*}, Shuhei Kurita^{3,5}, Koya Sakamoto^{6,4},
Daichi Azuma⁷, Yutaka Matsuo², Nakamasa Inoue¹

¹Tokyo Institute of Technology, ²The University of Tokyo, ³NII, ⁴ATR,
⁵RIKEN AIP ⁶Kyoto University ⁷Sony Semiconductor Solutions

Abstract

Vision-and-language navigation (VLN) aims to guide autonomous agents through real-world environments by integrating visual and linguistic cues. While substantial progress has been made in understanding these interactive modalities in ground-level navigation, aerial navigation remains largely underexplored. This is primarily due to the scarcity of resources suitable for real-world, city-scale aerial navigation studies. To bridge this gap, we introduce CityNav, a new dataset for language-goal aerial navigation using a 3D point cloud representation from real-world cities. CityNav includes 32,637 natural language descriptions paired with human demonstration trajectories, collected from participants via a new web-based 3D simulator developed for this research. Each description specifies a navigation goal, leveraging the names and locations of landmarks within real-world cities. We also provide baseline models of navigation agents that incorporate an internal 2D spatial map representing landmarks referenced in the descriptions. We benchmark the latest aerial navigation baselines and our proposed model on the CityNav dataset. The results using this dataset reveal the following key findings: (i) Our aerial agent models trained on human demonstration trajectories outperform those trained on shortest path trajectories, highlighting the importance of human-driven navigation strategies; (ii) The integration of a 2D spatial map significantly enhances navigation efficiency at city scale. Our dataset and code are available at <https://water-cookie.github.io/city-nav-proj/>.

1 Introduction

In the rapidly evolving field of Vision-and-Language Navigation (VLN) [3, 23], the integration of linguistic cues with visual data has opened new frontiers in autonomous navigation systems. Recently, significant progress has been made in the development of VLN datasets across varied environments from indoor house scenes [20, 24, 28, 37, 50] to outdoor urban scenes [7, 16, 33], including robotics applications [2, 43]. However, these datasets have primarily been designed for ground-level navigation towards home-assistance robots and autonomous vehicles. Consequently, the extension of VLN into an aerial domain has not been well explored. Unlike ground-level navigation, aerial navigation introduces unique challenges, such as vast 3D navigation spaces and the scarcity of datasets incorporating real-world data. The lack of comprehensive datasets and benchmarks for aerial VLN has hindered progress in this area and further advancements in unmanned aerial vehicle (UAV) applications such as drone delivery, 3D search-and-rescue, and disaster risk assessment.

A handful of studies have begun to explore aerial navigation, but they often rely on less realistic data sources that limit their applicability in real-world scenarios. Fan et al. [12] used satellite imagery for

*equal contribution



Figure 1: **CityNav dataset for language-goal aerial navigation.** The aerial agent is randomly spawned in the city and must find the target object corresponding to a given linguistic description. The agent’s ground truth trajectory, represented by the green line, was collected via crowd-sourcing services where participants used both the agent’s first-person view and a 2D map for navigation. In this case, the participant searched for the target object along the street, guided by geographical information.

aerial navigation, sparking advancements in aerial VLN agents despite overlooking 3D geometries in actual UAV flights. Similarly, Liu et al. [30] used data from virtual urban environments created by game engines, which allowed for diverse 3D maneuvers while sacrificing the complexity and realism of urban landscapes, as seen in point clouds scanned in the real-world, thereby limiting their geographical applicability. These studies highlight the need for more realistic and comprehensive datasets and benchmarks that better represent the challenges faced in aerial VLN.

In this work, we introduce CityNav, a dataset for language-goal aerial navigation at a city scale, designed to develop an intelligent aerial agent capable of locating specific geographical objects in real-world cities based on natural language descriptions. The dataset provides descriptions for city-scale point cloud data of SensatUrban [17], as well as their corresponding trajectories for training aerial agents. To collect large amounts of trajectories in photorealistic 3D environments, we implemented a web-based flight simulator synchronized with world maps. Figure 1 illustrates an example of our 3D flight simulator and a collected trajectory. In this simulator, users operate the aerial agent with six degrees of freedom through a continuous 3D state space to reach a destination that matches a language-goal description. Unlike previous works [12, 30], we utilized 3D scans of real cities to collect human-generated trajectories that consider geographic information in the map. Such geo-aware trajectories enable the aerial navigation model to narrow down the exploration space efficiently. In total, we acquired 32K trajectories corresponding to natural language descriptions about 5.8K objects (e.g., buildings and cars), which are approximately four times the size of the existing aerial VLN dataset [30]. To the best of our knowledge, the CityNav dataset represents the first large-scale 3D aerial navigation effort that leverages real-world 3D city data and contains a large amount of human-collected geo-aware trajectories and textual descriptions. Overall, our primary contributions are:

- **City-scale 3D aerial navigation dataset using real cities:** We provide a novel dataset for aerial navigation that follows language-goal descriptions using 3D scans of real cities. These descriptions incorporate geographical information obtained by filtering the city-scale 3D visual grounding

Table 1: Comparison with existing vision-and-language navigation datasets. Real: whether the environment is real-world data or not. N_{traj} : number of trajectories. L_{traj} : total trajectory length. Instruct.: granularity of instructions. Geo: availability of geographical data.

	Dataset	Real	N_{traj}	L_{traj}	Place	Instruct.	Environment	Geo
Ground	REVERIE [37]	Yes	7,234	72.3K	Indoor	Coarse	Matterport3D [5]	-
	R2R [3]	Yes	7,189	71.9K	Indoor	Fine	Matterport3D [5]	-
	R×R [24]	Yes	13,992	0.2M	Indoor	Coarse	Matterport3D [5]	-
	VLN-CE [23]	Yes	4,475	49.7K	Indoor	Coarse	Matterport3D [5]	-
	TouchDown [7]	Yes	9,326	2.9M	Outdoor	Fine	Google Street View	No
Aerial	LANI [34]	No	6,000	0.1M	Outdoor	Coarse	CHALET [52]	No
	AVDN [12]	Yes	3,064	0.9M	Outdoor	Dialog	xView [25]	No
	AerialVLN [30]	No	8,446	5.6M	Outdoor	Fine	Microsoft AirSim [44]	No
	CityNav (Ours)	Yes	32,637	17.8M	Outdoor	Coarse	SensatUrban [17]	Yes

dataset [35]. Additionally, we have collected a large amount of geo-aware trajectories by creating a web-based 3D flight simulator.

- **Geo-aware aerial vision-and-language navigation model:** We propose a baseline system that performs city-scale aerial navigation using a semantic map, which translates landmark text and semantic categories of geographic objects. Unlike previous methods, we used real-world map data to guide the agent toward the target object, in addition to using the agent’s observed images.
- **Benchmarking map-based vs. map-less aerial navigation methods:** We benchmark baseline methods on our dataset and demonstrate that our map-based method outperforms the existing map-less method, which simply learns from human-generated trajectories using imitation learning.

2 Related Work

VLN is a navigation task guiding an agent to a destination using both linguistic instructions and the agent’s visual observations. To benchmark this task, Embodied AI communities have devoted much effort into creating various VLN datasets. Table 1 presents the representative VLN datasets, which can be roughly categorized into ground-level and aerial navigation.

Ground-level navigation datasets. Recent advancements in 3D scanning technologies have significantly enhanced the ability to create highly accurate and photorealistic datasets of indoor 3D scenes [5, 8, 38, 41, 54]. Building on these indoor scene datasets, a wide range of VLN datasets, including robotics applications, has been proposed such as vision-and-language navigation [3, 19, 23, 24, 39], embodied referring expression [37], embodied question answering [9, 50, 55], vision-and-dialog navigation [36, 47] and daily-life tasks [46]. In outdoor environments, images from Google Street View are often utilized instead of 3D data. These images capture a wide variety of roadside views and landscapes from around the world. For example, TouchDown [7] is a dataset designed for studying natural language navigation and spatial reasoning in a real-world visual urban environment. It consists of 9,326 examples of instructions paired with human demonstrations to reach a goal in the Google Street View environment. Talk2Nav [48] is a dataset that contains verbal navigation instructions for 10,714 trajectories collected in an interactive visual navigation environment based on Google Street View. Ground-level navigation in both indoor and outdoor scenes searches a predetermined route, resulting in a narrow search area compared to the aerial domain.

Aerial navigation datasets. While the majority of VLN datasets primarily address ground-level navigation tasks, our work focuses on the more complex domain of aerial navigation, which presents unique challenges, including indeterminate routes and an expansive 3D search space that must be navigated. Initially, aerial navigation relied on the Global Navigation Satellite System (GNSS) and visual sensors to ensure safe and efficient flight in the vast and unconstrained aerial space [4, 18, 40, 45]. These systems are effective but can struggle in areas where GNSS is unreliable or unavailable. Progressing from these approaches, the vision-based approach uses machine learning to process visual data, allowing UAVs to adapt quickly to changes such as new weather conditions, unexpected obstacles, or altered landscapes [11, 13, 14, 22, 31]. The latest development integrates natural connection processing with vision, enabling UAVs to understand and execute commands that incorporate visual references and linguistic instructions, thereby facilitating more complex and

interactive tasks. However, the availability of such datasets in this field remains limited. LANI [34] is the initial dataset designed to evaluate UAV operations controlled by linguistic navigation instructions. The corresponding UAV’s 6,000 trajectories are obtained in the virtual environment CHALET [52], which is far from photorealistic, and the navigation environment is relatively small. Recent aerial navigation studies have increasingly expanded to outdoor environments, covering a broader range of areas. For flight simulation, the AVDN dataset [12], containing 3,064 aerial navigation trajectories with human-human dialog, uses the satellite images from the xView dataset [25], covering both urban and rural scenes. These satellite images, not captured by UAVs, result in limited clarity of geographical features and thus fail to simulate realistic environments for aerial navigation. As a more flexible setting, AerialVLN [30] performs the aerial VLN task using a 3D simulator of 25 city scenarios, supporting continuous state navigation. It includes 8,446 trajectories collected in virtual city environments of game engines by experienced human UAV pilots. In contrast, our proposed CityNav utilizes 3D point cloud data from SensatUrban [17] as UAV flight environments, consisting of 3D scans of real-world urban areas. Additionally, we used linguistic annotations and a 3D map with geographical information from the CityRefer dataset [35] as language-goal information and collected 32,637 human-generated trajectories corresponding to these descriptions, which are significantly larger than previous aerial VLN datasets.

3 CityNav Dataset

Our aerial navigation task aims to locate the target object based on the linguistic description and the agent’s first-person view images. For the descriptions, we used the filtered CityRefer dataset [35], which provides textual annotations for geographical objects in urban scenes from the SensatUrban dataset [17]. Similar to a previous aerial VLN task [30], the aerial agent is spawned at a random location within an outdoor environment, either previously encountered (seen) or new (unseen). The agent is tasked with the continuous exploration of the 3D environment until it successfully locates the target object. To achieve this, we employed imitation learning to train the navigation policy of an aerial agent. We created a web-based 3D flight simulator that integrates with Amazon Mechanical Turk (MTurk), detailed in Section 3.1, for collecting a substantial amount of human demonstrations. Subsequently, we describe the data collection via MTurk and outline the dataset’s quality control in Section 3.2. Finally, we analyze our CityNav dataset in Section 3.3.

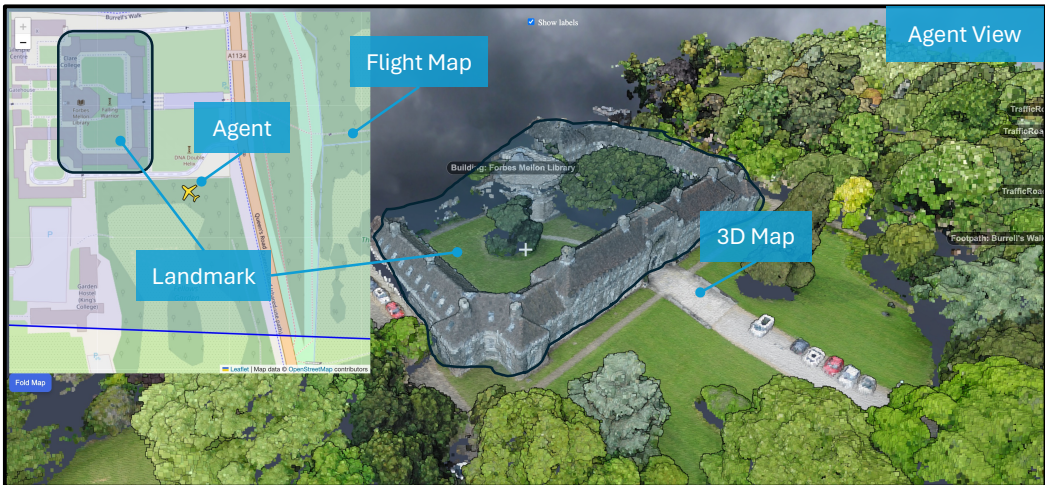


Figure 2: **3D flight simulator.** The user can utilize a flight map displayed in the top-left corner for efficient navigation, using geographic information from maps as clues.

3.1 Web-based 3D flight simulation

Flight simulator. To collect trajectory data via the web, we developed a web-based flight simulator that allows users to operate an aerial agent within 3D environments. This simulator uses Potree [42], an open-source WebGL-based point cloud renderer, to animate large-scale 3D scenes directly in the

browser, as illustrated in Figure 2. Potree features a first-person controller for intuitive navigation, enabling users to explore the 3D space. Users can move the agent forward, backward, left, right, up, and down using the keyboard and the mouse to change the agent’s direction. The simulator also includes a flight map linked to OpenStreetMap, which updates the agent’s real-time location.

Trajectory collection interface. We integrated the flight simulator with an MTurk interface to collect human demonstrations (i.e., trajectories) for aerial agents, which consists of a sequence of agent pose $[x, y, z, \hat{x}, \hat{y}, \hat{z}]$, where (x, y, z) denotes the agent’s position and $(\hat{x}, \hat{y}, \hat{z})$ denotes a unit vector of the agent’s orientation. For all episodes, the agents are placed in a 3D space at completely random positions on the XY-axis and 100-150 m on the Z-axis. Figure 3 illustrates the MTurk interface used to collect trajectories for the aerial VLN task. Participants were shown the aerial agent’s first-person perspective of the environment along with a description (e.g., “This is a black car on Chesterton Road on the side nearest the River Cam. It is near JSG Wine Merchant, has a blue car behind it, and a white car in front of it.”). They should operate the aerial agent to search for a specified object (e.g., “car,” “building,” or “parking lot”) within a given 3D scene, navigate to its location by controlling the agent’s movements, and place a marker in the center above the target. We considered that navigation was successful when the marker could be placed near the destination. The interface continuously collects the agent’s movement data in the background. After submitting the results, users could see the navigation score (ranging from 0 to 100, where higher is better) and the distance to goal (distance between the marker and the target, where lower is better) as feedback on the quality of the navigation.



Figure 3: **Trajectory collection interface:** Screenshot of the MTurk interface used for collecting human demonstrations after placing a marker.

3.2 Data Collection

Instruction. We instructed MTurk workers to control the aerial agent with the aim of locating the target object using the following guidelines:

You are the pilot of a flying object. The description of the 3D object will be displayed, and please find the target object on the 3D map by manipulating the flying object. Once you find the target object, get as close to the front of the object as you can within your field of vision, and then place a marker.

- Click on the 3D map to enable keyboard control of the flying object.
- Keyboard operation instructions are listed under the CONTROLS section.
- The description of the 3D object is mentioned in the “target object.”
- Your current location is displayed on the 2D map in the top left.
- You can drag, zoom in, and zoom out on the 2D map.
- Place a marker above the center of the target before submitting. Note that you cannot replace the marker.
- The description may contain information about landmarks. Use this in conjunction with the geographic information on the 2D map to gauge your destination.

In the first round, we collected trajectories corresponding to each description in the CityRefer dataset [35], which comprises 35,196 descriptions of 5,866 objects (each object is annotated with six different descriptions) across 34 scenes.

Quality control. To maintain the integrity of the aerial navigation data, we conducted filtering and re-collected the trajectories. During data collection, we decided not to assign any further tasks to participants who consistently recorded long distances to the goal or who did not move their agents from the starting point. After initial data collection, trajectories with a distance to the goal

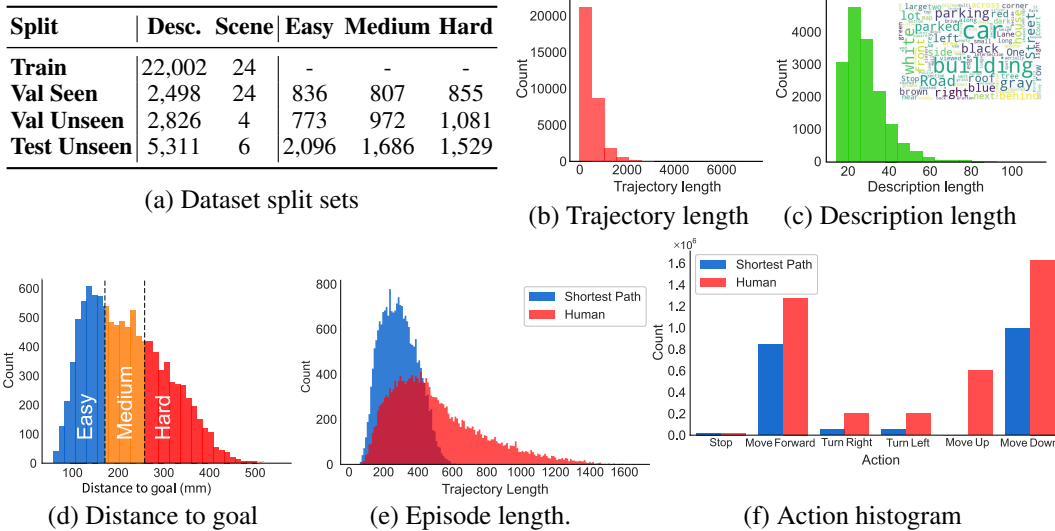


Figure 4: Statistics of the CityNav dataset.

greater than 30 m were excluded, obtaining a total of 81.6% trajectories. We then re-collected trajectories for the corresponding discarded data. Furthermore, in the re-collected data, 39.1% of the trajectories exceeding 30 m were again removed to use only those achievable trajectories for evaluation and training the agent’s navigation policy. Finally, we collected 32,637 pairs of descriptions and trajectories for 5,850 objects using our web-based simulator, which corresponds to 92.8% of the descriptions in the CityRefer dataset.

Data collection was conducted using MTurk, which required a total of 711 hours of labor at an estimated hourly rate of \$12.83, amounting to a total expenditure of \$9,123. A total of 171 users participated in the study.

3.3 Dataset Statistics

Dataset splits. Following previous studies [12, 30], we divided our dataset into four sets: ‘Train,’ ‘Val Seen,’ ‘Val Unseen,’ and ‘Test.’ The Val Seen set shares the scene with the training set, whereas the Val Unseen do not. The Val Seen and Train sets were created so that the corresponding objects do not overlap in their descriptions. Figure 4 (a) summarizes the statistics of the number of scenes and trajectories for each set.

Trajectory and description lengths. Figure 4 (b) illustrates the distributions for the length of collected trajectories. Figure 4 (c) illustrates the distributions for the description length corresponding to the trajectories. The figure at the top right corner displays frequent words of descriptions indicating a wide variety of vocabulary used for our aerial navigation task.

Difficulty levels. To evaluate tasks by difficulty level, we further divided the evaluation data (‘Val Unseen,’ ‘Val Seen,’ and ‘Test’) into Hard, Medium, and Easy sets. We defined the task difficulty based on the distance from the start position to the goal because a larger goal from the start of navigation requires more extensive exploration. We divided the evaluation sets according to the percentile of the distance in the training set, where the 33rd percentile for distance was 171 meters, and the 66th percentile was 258 meters. Figure 4 (d) shows the distance distribution of evaluation sets from the starting point to the goal. Episodes were categorized as ‘Easy’ for distances less than 171 m, ‘Medium’ for distances ranging from 171 to 258 m, and ‘Hard’ for distances exceeding 258 m. Figure 4 (a) shows the dataset statistics by difficulty. Unless specified otherwise, we used the Val Unseen set for evaluation.

Shortest paths and human demonstrations. We created a set of trajectories based on the shortest paths to compare them with human demonstrations. These shortest path trajectories are commonly used to train navigation modules in tasks such as Object Navigation [6] and Embodied Question Answering [9, 50]. We set the initial position to match the human demonstrations and generated the shortest path trajectories as a straight line connecting the initial position to the target object,

resulting in 32,637 trajectories. Following the AerialVLN [30], we generated ground-truth actions of a “look-ahead” path using the shortest path and human demonstration trajectories for imitation learning. Figure 4 (e) shows the episode length of both the shortest path and human demonstration trajectories. Human demonstration trajectories of the look-ahead path were longer than the shortest path (508 vs. 290 meters, on average). Figure 4 (f) shows action histograms for the shortest path and human demonstrations. Human demonstrations contain more Turn Left/Right and Move Up commands illustrating that they contain diverse trajectories.

4 Experiments

4.1 Experimental Setup

Evaluation. We measured the navigation performance with four standard evaluation metrics of VLN tasks [3, 30, 37]: navigation error (NE), success rate (SR), oracle success rate (OSR), and success weighted by path length (SPL). NE represents the navigation error in meters from the goal to the stopping point at termination. SR represents the success rate across all episodes, where success is defined as the agent stopping within 20 m of the destination. OSR measures the percentage of episodes where the distance on the xy-plane from any point on the trajectory to the target location is less than 20 m. SPL represents the success values weighted by the total length of the navigation trajectory [1].

Agent models. We implemented the following navigation models and compared them to our proposed model on the CityNav dataset. Further details of models and training are described in the Appendix.

- **Random** is a non-learning baseline, we provide a random agent that samples actions according to the action distribution of the training split of the human-collected trajectories.

- **Sequence-to-Sequence The(Seq2Seq)** [3] is a recurrent policy that predicts the next action based on the current RGB-D observation and descriptions. At each time step, the current-step RGB and depth images are encoded with pre-trained ResNet50 [15], and the description is encoded with an LSTM. The encoded embeddings then pass through a GRU and a feed-forward layer to output an action.

- **Cross-Modal Attention (CMA)** [3] extends the Seq2Seq model by introducing cross-modal attention features into the decision-making process. In addition to RGB, depth, and description embeddings, the model computes attention of description and visual features, which are computed by applying scaled dot-product attention [49]. Based on these features, CMA predicts the next action. The latest work in aerial VLN utilizes this model [30].

- **Map-based Goal Predictor (MGP)** is our proposed model that combines state-of-the-art off-the-shelf models to perform map-based goal prediction. As shown in Figure 5, it utilizes navigation maps generated at each time step through the following three steps: (i) target, landmark, and surroundings name extraction by GPT-3.5 Turbo, (ii) object detection and segmentation using GroundingDINO [29] and Mobile-SAM [56], and (iii) optional coordinate refinement by LLaVA-1.6-34b [27]

using the set-of-mark prompting [53]. A map encoder, using a navigation map that includes a landmark map, view & explore area maps, and target & surroundings maps, was trained alongside the RGB and depth encoders of CMA. Further details are provided in the Appendix.

Implementation details. The Seq2Seq and CMA models were trained using the Adam optimizer [21] for 5 epochs with a learning rate set to 1.5×10^{-3} and a batch size of 12. The MGP model was trained with the AdamW optimizer [32] for 10 epochs with a learning rate of 1.0×10^{-3} and a batch size of 8.

4.2 Experimental Results

Overall performance. Table 2 shows the overall aerial navigation results for the evaluation sets on the CityNav dataset. Among the navigation agents, our MGP agents using navigation maps outperformed the other agents in all four metrics across all evaluation sets. This suggests that geographical map

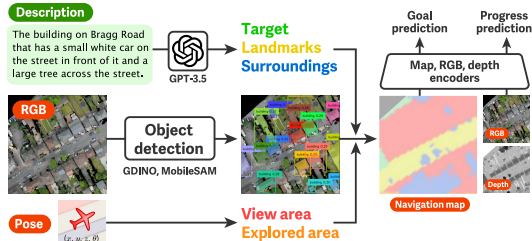


Figure 5: Overview of map-based goal predictor

Table 2: Overall aerial navigation performance. Learning-based models are evaluated with shortest path (SP) or human demonstrations (HD) trajectories.

Method	Validation Seen				Validation Unseen				Test Unseen			
	NE↓	SR↑	OSR↑	SPL↑	NE↓	SR↑	OSR↑	SPL↑	NE↓	SR↑	OSR↑	SPL↑
Random	222.3	0.00	1.15	0.00	223.0	0.00	0.90	0.00	208.8	0.00	1.44	0.00
Seq2Seq w/ SP	148.4	4.52	10.61	4.47	201.4	1.04	8.03	1.02	174.5	1.73	8.57	1.69
Seq2Seq w/ HD	257.1	1.81	7.89	1.58	317.4	0.79	8.82	0.61	245.3	1.50	8.34	1.30
CMA w/ SP	151.7	3.74	10.77	3.70	205.2	1.08	7.89	1.06	179.1	1.61	10.07	1.57
CMA w/ HD	240.8	0.95	9.42	0.92	268.8	0.65	7.86	0.63	252.6	0.82	9.70	0.79
MGP w/ SP	76.0	5.56	22.22	5.36	95.6	3.57	14.47	3.51	110.0	4.46	17.00	4.32
MGP w/ HD	60.9	7.21	34.79	6.59	75.3	5.02	21.90	4.67	94.4	5.57	25.80	5.25
MGP+LLaVA w/ SP	75.0	6.53	22.26	6.27	93.4	4.32	15.00	4.24	109.0	4.73	17.47	4.62
MGP+LLaVA w/ HD	59.7	8.69	35.51	8.28	75.1	5.84	22.19	5.56	93.8	6.38	26.04	6.08
Human	9.1	89.31	96.40	60.17	9.4	88.39	95.54	62.66	9.8	87.86	95.29	57.04

Table 3: Aerial navigation performance across difficulty levels. Human demos are used for training.

Method	Easy				Medium				Hard			
	NE↓	SR↑	OSR↑	SPL↑	NE↓	SR↑	OSR↑	SPL↑	NE↓	SR↑	OSR↑	SPL↑
Random	127.5	0.00	3.60	0.00	212.0	0.00	0.00	0.00	319.8	0.00	0.00	0.00
Seq2Seq	238.8	3.07	14.70	2.64	246.5	0.43	3.87	0.38	253.1	0.48	4.38	0.44
CMA	260.7	0.49	16.69	0.44	241.2	1.10	7.67	1.09	253.8	0.96	1.64	0.95
MGP	99.3	5.49	40.31	4.80	91.3	6.23	21.41	6.08	91.0	4.97	10.73	4.94
MGP+LLaVA	98.9	6.15	39.89	5.48	90.9	6.29	21.47	6.21	90.0	6.80	12.10	6.78
Human	9.4	88.45	95.85	55.80	9.8	87.54	95.26	56.54	10.1	87.38	94.57	59.30

information is crucial for enhancing the accuracy of the aerial VLN task with the real city dataset, which encompasses a large search space. However, we observed that the manual navigation (Human) significantly outperformed other navigation agent models. Even the MGP agents, which utilized state-of-the-art off-the-shelf models, were approximately ten times less likely to succeed in the task compared to the manual navigation. This indicates that the CityNav task requires more sophisticated planning and complex spatial reasoning capabilities to perform on par with humans.

Shortest paths vs. human demonstrations. Table 2 shows that the MGP agents performed better when trained with human demonstration trajectories than with automatically generated shortest-path ones. We believe this result suggests that the navigation map aids in deciphering the complex relationship between the instruction and the corresponding human demonstrations.

Difficulty by distance to target. Table 3 shows the navigation performance across three difficulty levels. The agents that did not use maps (Random, Seq2Seq, and CMA) showed lower performance on the medium and hard sets compared to the easy set. In contrast, our MGP agents and humans displayed more consistent results across the sets, confirming that map information plays an

Table 4: Performance by training size (MGP+LLaVA).

Path	Size	NE ↓	SR ↑	OSR ↑
SP	1k	83.8	4.41	13.88
SP	8k	80.5	4.27	14.56
SP	22k	93.4	4.32	15.00
HD	1k	83.4	4.30	23.10
HD	8k	80.9	4.41	18.69
HD	22k	75.1	5.84	22.19

important role in the successful completion of the aerial navigation task.

Effect of the number of human demonstrations. In Table 4, we compared how changing the training dataset size affected the performance. We found that increasing the number of human demonstrations improved the navigation error and success rate while increasing the number of shortest paths did not show a consistent trend.

Ablation study. Table 5 shows the success rate of MGP+LLaVA when some of the channels in the internal map representation were ablated. We observed that the success rate dropped to 0.47% when the landmark map was not provided, which agrees with our assumption that the ability to connect named objects mentioned in descriptions to the

Table 5: Ablation study.

Method	SR ↑
MGP+LLaVA	5.84
w/o landmark map	0.47
w/o view & explored area maps	5.49
w/o target & surroundings maps	5.81

spatial 2D map is critical for the task. We also found that the target & surroundings maps make only a small contribution to the performance. This is likely due to the difference in camera perspectives between the training data of the Grounding-DINO and the observation images in the task.

Qualitative results. Figure 6 illustrates successful examples of the proposed aerial navigation model (MGP) when incorporating landmark map information. The examples demonstrate how geographic information helps to locate target objects. In the leftmost example, the aerial agent moves forward from the spawned location along ‘Hobson Street’ based on the given description. Then, the agent found ‘Stevenson Building’ and located three cars next to it. The center example shows that the aerial agent took action to recognize ‘The Avenue Footpath’ and ‘The Garret Hostel Lane Footpath’ to locate the green field area between both streets. The rightmost example shows the agent’s trajectory when the linguistic information is more complicated. Initially, the aerial agent moved along the street and found the intersection between ‘The Pound Hill Road’ and ‘Northampton Street,’ The agent missed the building mentioned in the description, but after finding ‘Castle Street,’ it corrected its course and successfully located the correct buildings. These examples suggest that aligning the described geographic information with real-world maps could lead to further enhancements in navigation efficiency.



Figure 6: Qualitative examples.

5 Conclusion

This paper presents CityNav, a city-scale aerial VLN dataset containing 32,637 descriptions paired with human-generated trajectories about 5,850 geographical objects in real cities. We benchmarked current aerial VLN models against our map-based goal prediction model on this dataset. Experimental results demonstrated that the proposed model, which utilizes 2D spatial map representations and human-generated geo-aware trajectories, enhances navigation performance. We believe our CityNav dataset could be a valuable resource for benchmarking and training intelligent aerial agents.

Limitations and Future Work. The CityNav dataset does not account for agent-object interaction and dynamic elements like moving vehicles and pedestrians in urban simulations. Addressing this could enhance realism and applicability in real-world scenarios. Future work could include integrating physical interaction and real-time data to improve navigation accuracy and expand the dataset.

Broader Impacts. CityNav can potentially improve tasks like urban surveillance and emergency response by enabling aerial agents to navigate via natural language. However, these technologies also raise ethical concerns, regarding privacy and data security. It is crucial to consider social acceptance and regulatory issues, engage with communities to ensure equitable benefits, and address potential risks to privacy and safety.

Acknowledgements

This work was supported by JST PRESTO Grant Number JPMJPR22P8, and JSPS KAKENHI Grant Numbers JP22K12159, JP22K17983, JP22KK0184, Japan. This research project has benefitted from the Microsoft Accelerate Foundation Models Research (AFMR) grant program through which leading foundation models hosted by Microsoft Azure along with access to Azure credits were provided to conduct the research.

References

- [1] P. Anderson, A. Chang, D. Chaplot, A. Dosovitskiy, S. Gupta, V. Koltun, J. Košecká, J. Malik, R. Mottaghi, M. Savva, and A. Zamir. On evaluation of embodied navigation agents. *arXiv preprint arXiv:1807.06757*, 2018.
- [2] P. Anderson, A. Shrivastava, J. Truong, A. Majumdar, D. Parikh, D. Batra, and S. Lee. Sim-to-real transfer for vision-and-language navigation. In *Proceedings of the Conference on Robot Learning (CoRL)*, pages 671–681, 2020.
- [3] P. Anderson, Q. Wu, D. Teney, J. Bruce, M. Johnson, N. Sünderhauf, I. Reid, S. Gould, and A. van den Hengel. Vision-and-language navigation: Interpreting visually-grounded navigation instructions in real environments. In *Proceedings of the IEEE/CVF Conference on Computer Vision and Pattern Recognition (CVPR)*, pages 3674–3683, 2018.
- [4] A. Chambers, S. Achar, S. Nuske, J. Rehder, B. Kitt, L. Chamberlain, J. Haines, S. Scherer, and S. Singh. Perception for a river mapping robot. In *Proceedings of the IEEE/RSJ International Conference on Intelligent Robots and Systems (IROS)*, pages 227–234, 2011.
- [5] A. Chang, A. Dai, T. Funkhouser, M. Halber, M. Niebner, M. Savva, S. Song, A. Zeng, and Y. Zhang. Matterport3D: Learning from RGB-D data in indoor environments. In *Proceedings of the International Conference on 3D Vision (3DV)*, pages 667–676, 2017.
- [6] D. S. Chaplot, D. Gandhi, A. Gupta, and R. Salakhutdinov. Object goal navigation using goal-oriented semantic exploration. In *Proceedings of the Annual Conference on Neural Information Processing Systems (NeurIPS)*, pages 671–681, 2020.
- [7] H. Chen, A. Suhr, D. Misra, N. Snavely, and Y. Artzi. Touchdown: Natural language navigation and spatial reasoning in visual street environments. In *Proceedings of the IEEE/CVF Conference on Computer Vision and Pattern Recognition (CVPR)*, pages 12538–12547, 2019.
- [8] A. Dai, A. X. Chang, M. Savva, M. Halber, T. Funkhouser, and M. Nießner. Scannet: Richly-annotated 3d reconstructions of indoor scenes. In *Proceedings of the IEEE/CVF Conference on Computer Vision and Pattern Recognition (CVPR)*, pages 5829–5839, 2017.
- [9] A. Das, S. Datta, G. Gkioxari, S. Lee, D. Parikh, and D. Batra. Embodied Question Answering. In *Proceedings of the IEEE/CVF Conference on Computer Vision and Pattern Recognition (CVPR)*, pages 1–10, 2018.
- [10] J. Deng, W. Dong, R. Socher, L.-J. Li, K. Li, and L. Fei-Fei. Imagenet: A large-scale hierarchical image database. In *Proceedings of the IEEE/CVF Conference on Computer Vision and Pattern Recognition (CVPR)*, pages 248–255, 2009.
- [11] G. Dhiraj, L. Pinto, and A. Gupta. Learning to fly by crashing. In *Proceedings of the IEEE/RSJ International Conference on Intelligent Robots and Systems (IROS)*, page 3948–3955, 2017.
- [12] Y. Fan, W. Chen, T. Jiang, C. Zhou, Y. Zhang, and X. E. Wang. Aerial vision-and-dialog navigation. In *Findings of the Association for Computational Linguistics (ACL Findings)*, pages 3043–3061, 2023.
- [13] F. Fraundorfer, L. Heng, D. Honegger, G. H. Lee, L. Meier, P. Tanskanen, and M. Pollefeys. Vision-based autonomous mapping and exploration using a quadrotor mav. In *Proceedings of the IEEE/RSJ International Conference on Intelligent Robots and Systems (IROS)*, pages 4557–4564, 2012.
- [14] A. Giusti, J. Guzzi, D. C. Cireşan, F.-L. He, J. P. Rodríguez, F. Fontana, M. Faessler, C. Forster, J. Schmidhuber, G. Di Caro, et al. A machine learning approach to visual perception of forest trails for mobile robots. *IEEE Robotics and Automation Letters (RA-L)*, 1(2):661–667, 2015.
- [15] K. He, X. Zhang, S. Ren, and J. Sun. Deep residual learning for image recognition. In *Proceedings of the IEEE/CVF Conference on Computer Vision and Pattern Recognition (CVPR)*, pages 770–778, 2016.
- [16] K. M. Hermann, M. Malinowski, P. Mirowski, A. Banki-Horvath, K. Anderson, and R. Hadsell. Learning to follow directions in street view. In *Proceedings of the AAAI Conference on Artificial Intelligence (AAAI)*, pages 11773–11781, 2020.
- [17] Q. Hu, B. Yang, S. Khalid, W. Xiao, N. Trigoni, and A. Markham. Sensaturban: Learning semantics from urban-scale photogrammetric point clouds. *International Journal of Computer Vision (IJCV)*, 130:316–343, 2022.

- [18] A. S. Huang, A. Bachrach, P. Henry, M. Krainin, D. Maturana, D. Fox, and N. Roy. Visual odometry and mapping for autonomous flight using an rgb-d camera. In *Proceedings of the International Symposium of Robotics Research (ISRR)*, pages 235–252, 2017.
- [19] V. Jain, G. Magalhaes, A. Ku, A. Vaswani, E. Ie, and J. Baldridge. Stay on the path: Instruction fidelity in vision-and-language navigation. In *Proceedings of the Annual Meeting of the Association for Computational Linguistics (ACL)*, pages 1862–1872, 2019.
- [20] M. Khanna, R. Ramrakhya, G. Chhablani, S. Yenamandra, T. Gervet, M. Chang, Z. Kira, D. S. Chaplot, D. Batra, and R. Mottaghi. Goat-bench: A benchmark for multi-modal lifelong navigation. *arXiv preprint arXiv:2404.06609*, 2024.
- [21] D. P. Kingma and J. Ba. Adam: A method for stochastic optimization. In *Proceedings of the International Conference on Learning Representations (ICLR)*, 2015.
- [22] A. Kouris and C.-S. Bouganis. Learning to fly by myself: A self-supervised cnn-based approach for autonomous navigation. In *Proceedings of the IEEE/RSJ International Conference on Intelligent Robots and Systems (IROS)*, pages 1–9, 2018.
- [23] J. Krantz, E. Wijmans, A. Majundar, D. Batra, and S. Lee. Beyond the nav-graph: Vision and language navigation in continuous environments. In *European Conference on Computer Vision (ECCV)*, page 104–120, 2020.
- [24] A. Ku, P. Anderson, R. Patel, E. Ie, and J. Baldridge. Room-Across-Room: Multilingual vision-and-language navigation with dense spatiotemporal grounding. In *Proceedings of the Conference on Empirical Methods in Natural Language Processing (EMNLP)*, pages 4392–4412, 2020.
- [25] D. Lam, R. Kuzma, K. McGee, S. Dooley, M. Laielli, M. Klaric, Y. Bulatov, and B. McCord. xviv: Objects in context in overhead imagery. *arXiv preprint arXiv:1802.07856*, 2018.
- [26] F. Li, H. Zhang, P. Sun, X. Zou, S. Liu, J. Yang, C. Li, L. Zhang, and J. Gao. Semantic-sam: Segment and recognize anything at any granularity. *arXiv preprint arXiv:2307.04767*, 2023.
- [27] H. Liu, C. Li, Q. Wu, and Y. J. Lee. Visual instruction tuning. In *Proceedings of the Annual Conference on Neural Information Processing Systems (NeurIPS)*, pages 34892–34916, 2023.
- [28] H. Liu, A. Lin, X. Han, L. Yang, Y. Yu, and S. Cui. Refer-it-in-rgbd: A bottom-up approach for 3d visual grounding in rgbd images. In *Proceedings of the IEEE/CVF Conference on Computer Vision and Pattern Recognition (CVPR)*, pages 6032–6041, 2021.
- [29] S. Liu, Z. Zeng, T. Ren, F. Li, H. Zhang, J. Yang, C. Li, J. Yang, H. Su, J. Zhu, et al. Grounding dino: Marrying dino with grounded pre-training for open-set object detection. *arXiv preprint arXiv:2303.05499*, 2023.
- [30] S. Liu, H. Zhang, Y. Qi, P. Wang, Y. Zhang, and Q. Wu. AerialVLN: Vision-and-language navigation for uavs. In *Proceedings of the IEEE/CVF International Conference on Computer Vision (ICCV)*, pages 15384–15394, 2023.
- [31] A. Loquercio, A. M. I. Maqueda, C. R. del Blanco, and D. Scaramuzza. Dronet: Learning to fly by driving. *IEEE Robotics and Automation Letters (RA-L)*, 3:1088–1095, 2018.
- [32] I. Loshchilov and F. Hutter. Fixing weight decay regularization in adam. *arXiv preprint arXiv:1711.05101*, 2017.
- [33] P. Mirowski, M. K. Grimes, M. Malinowski, K. M. Hermann, K. Anderson, D. Teplyashin, K. Simonyan, K. Kavukcuoglu, A. Zisserman, and R. Hadsell. Learning to navigate in cities without a map. In *Proceedings of the Annual Conference on Neural Information Processing Systems (NeurIPS)*, 2018.
- [34] D. Misra, A. Bennett, V. Blukis, E. Niklasson, M. Shatkhin, and Y. Artzi. Mapping instructions to actions in 3d environments with visual goal prediction. In *Proceedings of the Conference on Empirical Methods in Natural Language Processing (EMNLP)*, pages 2667–2678, 2018.
- [35] T. Miyanishi, F. Kitamori, S. Kurita, J. Lee, M. Kawanabe, and N. Inoue. Cityrefer: Geography-aware 3d visual grounding dataset on city-scale point cloud data. In *Proceedings of the Annual Conference on Neural Information Processing Systems (NeurIPS)*, pages 77758–77770, 2023.
- [36] K. Nguyen and H. Daumé III. Help, Anna! visual navigation with natural multimodal assistance via retrospective curiosity-encouraging imitation learning. In *Proceedings of the Conference on Empirical Methods in Natural Language Processing and International Joint Conference on Natural Language Processing (EMNLP-IJCNLP)*, pages 684–695, 2019.

- [37] Y. Qi, Q. Wu, P. Anderson, X. Wang, W. Y. Wang, C. Shen, and A. van den Hengel. Reverie: Remote embodied visual referring expression in real indoor environments. In *Proceedings of the IEEE/CVF Conference on Computer Vision and Pattern Recognition (CVPR)*, 2020.
- [38] S. K. Ramakrishnan, A. Gokaslan, E. Wijmans, O. Maksymets, A. Clegg, J. M. Turner, E. Undersander, W. Galuba, A. Westbury, A. X. Chang, M. Savva, Y. Zhao, and D. Batra. Habitat-matterport 3d dataset (HM3d): 1000 large-scale 3d environments for embodied AI. In *Proceedings of the Annual Conference on Neural Information Processing Systems (NeurIPS)*, 2021.
- [39] R. Ramrakhya, E. Undersander, D. Batra, and A. Das. Habitat-web: Learning embodied object-search strategies from human demonstrations at scale. In *Proceedings of the IEEE/CVF Conference on Computer Vision and Pattern Recognition (CVPR)*, pages 5173–5183, 2022.
- [40] S. Ross, N. Melik-Barkhudarov, K. S. Shankar, A. Wendel, D. Dey, J. A. Bagnell, and M. Hebert. Learning monocular reactive uav control in cluttered natural environments. In *Proceedings of the IEEE International Conference on Robotics and Automation (ICRA)*, pages 1765–1772, 2013.
- [41] M. Savva, A. Kadian, O. Maksymets, Y. Zhao, E. Wijmans, B. Jain, J. Straub, J. Liu, V. Koltun, J. Malik, D. Parikh, and D. Batra. Habitat: A Platform for Embodied AI Research. In *Proceedings of the IEEE/CVF International Conference on Computer Vision (ICCV)*, pages 9339–9347, 2019.
- [42] M. Schütz et al. Potree: Rendering large point clouds in web browsers. *Technische Universität Wien, Wiedeń*, 2016.
- [43] D. Shah, B. Osiński, b. ichter, and S. Levine. Lm-nav: Robotic navigation with large pre-trained models of language, vision, and action. In *Proceedings of the Conference on Robot Learning (CoRL)*, pages 492–504, 2023.
- [44] S. Shah, D. Dey, C. Lovett, and A. Kapoor. Airsim: High-fidelity visual and physical simulation for autonomous vehicles. In *Proceedings of the Conference on Field and Service Robotics (FSR)*, page 621–635, 2017.
- [45] S. Shen, Y. Mulgaonkar, N. Michael, and V. Kumar. Multi-sensor fusion for robust autonomous flight in indoor and outdoor environments with a rotorcraft mav. In *Proceedings of the IEEE International Conference on Robotics and Automation (ICRA)*, pages 4974–4981, 2014.
- [46] M. Shridhar, J. Thomason, D. Gordon, Y. Bisk, W. Han, R. Mottaghi, L. Zettlemoyer, and D. Fox. ALFRED: A Benchmark for Interpreting Grounded Instructions for Everyday Tasks. In *The IEEE Conference on Computer Vision and Pattern Recognition (CVPR)*, pages 10740–10749, 2020.
- [47] J. Thomason, M. Murray, M. Cakmak, and L. Zettlemoyer. Vision-and-dialog navigation. In *Proceedings of the Conference on Robot Learning (CoRL)*, pages 394–406, 2020.
- [48] A. B. Vasudevan, D. Dai, and L. Van Gool. Talk2nav: Long-range vision-and-language navigation with dual attention and spatial memory. *International Journal of Computer Vision (IJCV)*, 129(1):246–266, 2021.
- [49] A. Vaswani, N. Shazeer, N. Parmar, J. Uszkoreit, L. Jones, A. N. Gomez, Ł. Kaiser, and I. Polosukhin. Attention is all you need. In *Proceedings of the Annual Conference on Neural Information Processing Systems (NeurIPS)*, 2017.
- [50] E. Wijmans, S. Datta, O. Maksymets, A. Das, G. Gkioxari, S. Lee, I. Essa, D. Parikh, and D. Batra. Embodied Question Answering in Photorealistic Environments with Point Cloud Perception. In *Proceedings of the IEEE/CVF Conference on Computer Vision and Pattern Recognition (CVPR)*, pages 6659–6668, 2019.
- [51] E. Wijmans, A. Kadian, A. Morcos, S. Lee, I. Essa, D. Parikh, M. Savva, and D. Batra. DD-PPO: Learning near-perfect pointgoal navigators from 2.5 billion frames. In *Proceedings of the International Conference on Learning Representations (ICLR)*, 2020.
- [52] C. Yan, D. Misra, A. Bennet, A. Walsman, Y. Bisk, and Y. Artzi. Chalet: Cornell house agent learning environment. *arXiv preprint arXiv:1801.07357*, 2018.
- [53] J. Yang, H. Zhang, F. Li, X. Zou, C. Li, and J. Gao. Set-of-mark prompting unleashes extraordinary visual grounding in GPT-4V. *arXiv preprint arXiv:2310.11441*, 2023.

- [54] C. Yeshwanth, Y.-C. Liu, M. Nießner, and A. Dai. Scannet++: A high-fidelity dataset of 3d indoor scenes. In *Proceedings of the International Conference on Computer Vision (ICCV)*, pages 12–22, 2023.
- [55] L. Yu, X. Chen, G. Gkioxari, M. Bansal, T. L. Berg, and D. Batra. Multi-target embodied question answering. In *Proceedings of the IEEE/CVF Conference on Computer Vision and Pattern Recognition (CVPR)*, pages 6309–6318, 2019.
- [56] C. Zhang, D. Han, Y. Qiao, J. U. Kim, S.-H. Bae, S. Lee, and C. S. Hong. Faster segment anything: Towards lightweight sam for mobile applications. *arXiv preprint arXiv:2306.14289*, 2023.

CityNav: Supplementary Material

This is supplementary material for the paper: *CityNav: Language-Goal Aerial Navigation Dataset with Geographic Information*. We present additional details of the data collection interface, models, and experimental results.

1 Interface Details

We developed the data collection website on the Amazon Mechanical Turk platform. Figure 7 shows the full screenshot of the data collection web interface that allows users to operate an aerial agent within 3D environments.

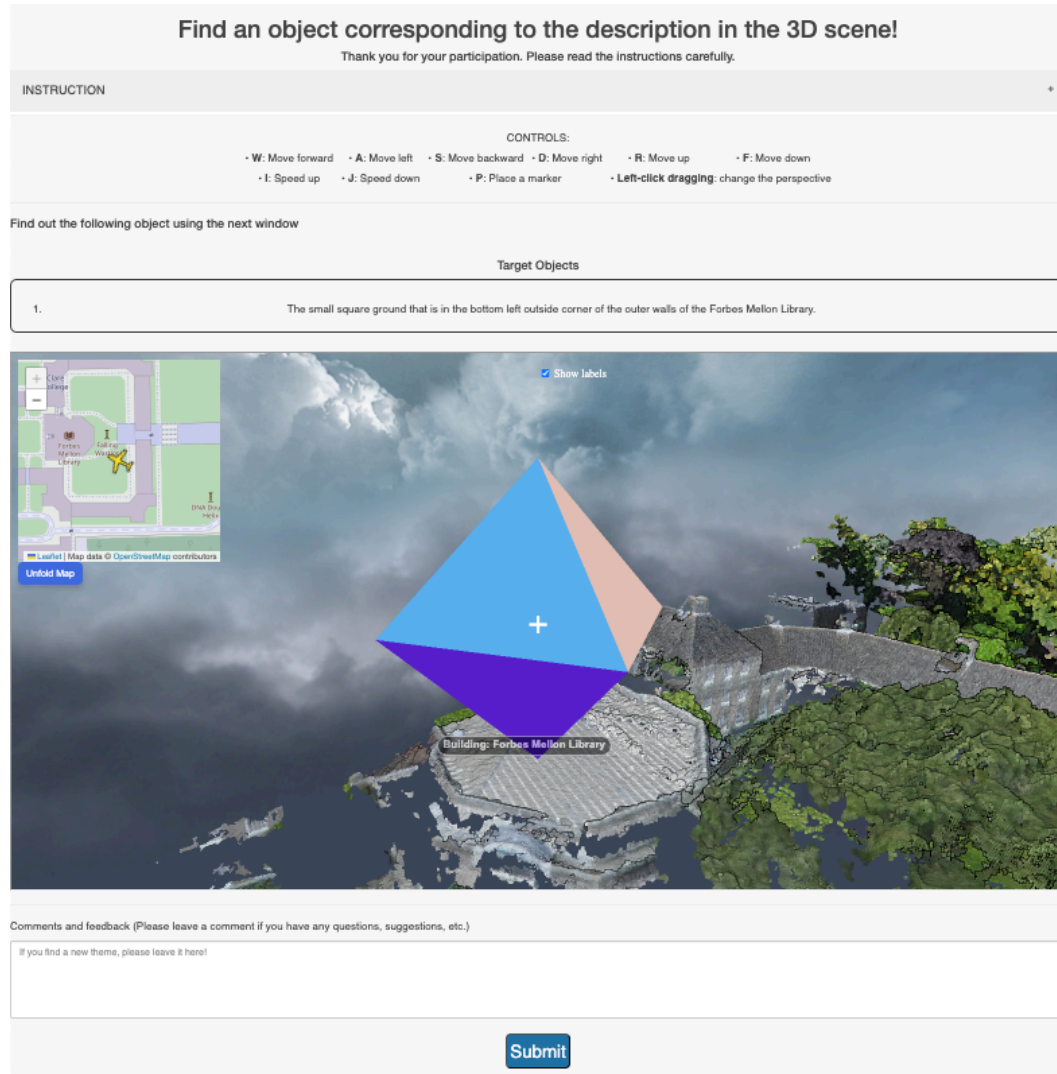


Figure 7: **Trajectory collection interface.** Full screenshot of web interface for collecting human demonstration trajectories for the CityNav dataset.

2 Agent Model Details

We provide additional architectural details of aerial agents for baseline agent models (Sequence-to-Sequence and Cross-Modal Attention) and our proposed model (Map-based Goal Predictor). The first two baselines do not use geographical information, while the latter proposed method uses geographical information for aerial navigation.

2.1 Sequence-to-Sequence

Sequence-to-Sequence (Seq2Seq) model [3] is a recurrent policy that predicts the next action based on the current RGB-D observation and descriptions. At each time step t , the RGB image $\mathbf{o}_{\text{RGB}}^t$, the depth image $\mathbf{o}_{\text{depth}}^t$ and the description $\mathbf{o}_{\text{instr}} = [\tau^1, \dots, \tau^L]$ are encoded into RGB, depth, and description embeddings. The RGB embedding $\mathbf{f}_{\text{RGB}}^t$ is obtained by extracting the features from the RGB observation using a ResNet50 [15] pretrained with ImageNet [10] and flattening the average-pooled features into a 256-dimensional vector. The depth embedding $\mathbf{f}_{\text{depth}}^t$ is computed similarly, but uses a ResNet50 trained on a point-goal navigation task [51] and flattens the features into a 128-dimensional vector without applying average pooling operations. To encode the description embedding $\mathbf{f}_{\text{instr}}$, the tokenized description is fed into an LSTM, and the final hidden state of dimension 128 is taken from the outputs. The embeddings are then concatenated to form a 512-dimensional input vector $[\mathbf{f}_{\text{RGB}}^t \ \mathbf{f}_{\text{depth}}^t \ \mathbf{f}_{\text{instr}}]$ to be fed into a GRU along with the previous hidden state \mathbf{h}^t . Finally, the output from the GRU is passed through a feed-forward layer to output the logits of the predicted action distribution.

2.2 Cross-Modal Attention

Cross-Modal Attention (CMA) model [3] extends the Seq2Seq model by introducing cross-modal attention features into the decision-making process. While the input embeddings stay mostly the same as Seq2Seq model, with the exception of the description embedding using all the intermediate hidden states $[\mathbf{f}_{\text{instr}}^1, \dots, \mathbf{f}_{\text{instr}}^L] = \text{BiLSTM}([\tau^1, \dots, \tau^L])$ from a bidirectional LSTM, the model computes attended visual features $\hat{\mathbf{f}}_{\text{RGB}}^t, \hat{\mathbf{f}}_{\text{depth}}^t$ and attended description features $\hat{\mathbf{f}}_{\text{instr}}$ to aid the reasoning of relative spatial references and focusing on relevant parts of the description. Attended description features are computed as $\hat{\mathbf{f}}_{\text{instr}} = \text{Attn}([\mathbf{f}_{\text{instr}}^1, \dots, \mathbf{f}_{\text{instr}}^L], \mathbf{h}_v^t)$, where Attn denotes a scaled dot-product attention [49] and $\mathbf{h}_v^t = \text{GRU}([\mathbf{f}_{\text{RGB}}^t, \mathbf{f}_{\text{depth}}^t, \mathbf{a}^{t-1}], \mathbf{h}_v^{t-1})$ is a recurrent representation of the visual observations calculated from RGB and depth embeddings $\mathbf{f}_{\text{RGB}}^t, \mathbf{f}_{\text{depth}}^t$ and a 32-dimensional embedding of the previous action \mathbf{a}^{t-1} . Attended visual features are then obtained by applying scaled dot-product attention between the visual features and the attended description features, which can be expressed as $\hat{\mathbf{f}}_{\text{RGB}}^t = \text{Attn}(\mathbf{f}_{\text{RGB}}^t, \mathbf{f}_{\text{instr}}^1), \hat{\mathbf{f}}_{\text{depth}}^t = \text{Attn}(\mathbf{f}_{\text{depth}}^t, \mathbf{f}_{\text{instr}}^1)$. The attended visual and description features, $\hat{\mathbf{f}}_{\text{RGB}}^t, \hat{\mathbf{f}}_{\text{depth}}^t, \hat{\mathbf{f}}_{\text{instr}}$, action embedding \mathbf{a}^{t-1} and the hidden state of the first GRU \mathbf{h}_v^t are all concatenated as the input to a second GRU and a feed-forward layer, producing the logit values for the predicted action distribution.

2.3 Map-based Goal Predictor

While the CMA model is designed to handle tasks involving spatial reasoning, it cannot inherently recognize named objects (e.g., “Willmore Road”), which is crucial for locating unnamed objects (e.g., a red car parked on the side of Willmore Road) in urban outdoor environments. To address this issue, we introduce a simple model called a map-based goal predictor, as shown in Figure 8.

The model outputs two values: predicted goal coordinates and predicted progress. The predicted goal coordinates guess the location of the target object based on previous observations. The predicted progress estimates the ratio of the remaining distance to the total distance from the starting point to the goal. To move toward the predicted coordinates, the agent updates the predicted goal coordinates based on the observations and executes up to five actions consecutively at each time step. When the value of the predicted progress exceeds a threshold, the agent stops iterating and moves directly to the predicted goal coordinates.

The predicted goal coordinates are computed based on a navigation map that keeps track of the locations of objects and structures relevant to the description. The navigation map itself is maintained

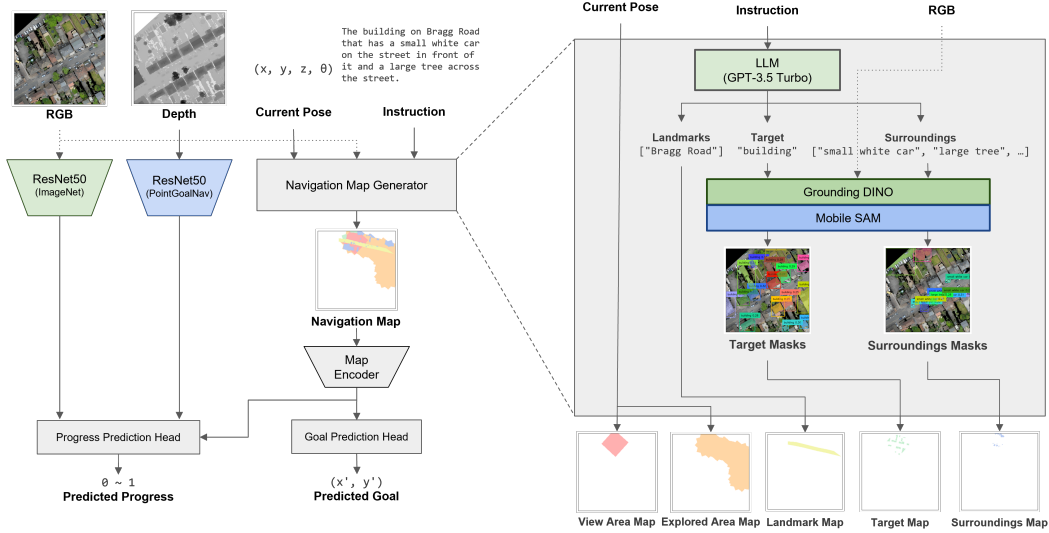


Figure 8: A detailed layout of the map-based goal predictor.

by the ‘Navigation Map Generator’ module shown on the right side of Figure 8. A navigation map consists of five channels, with the first two channels bookkeeping the navigation history and the rest of the channels recording where the entities within the description are located. The first channel, named *view area map*, represents the area that is currently being rendered in the RGB and depth image. The second channel *explored area map* is an aggregation of view area maps over time steps. The third, fourth, and fifth channels are *landmark map*, *target map* and *surroundings map*. These maps mark the entities mentioned in the description, where the names of the entities are extracted using ChatGPT-3.5 Turbo with few-shot prompting. The first type of entity is a *landmark*, which is a named structure whose exact location can be identified via online maps (e.g. “Grand Square”). Using the names and contour coordinates of landmarks provided by the CityRefer dataset [35], landmarks mentioned in the description are marked on the map. The second and third types of entity are *target* and *surroundings*, where a target is an entity being described by the description (e.g. “a building with a grey roof”) and surroundings are unnamed entities that appear in the description to the target (e.g. “a red van with black stripes”). Since the names of the target and surroundings are not confined to a predefined set of categories, we employ Grounding DINO [29], an open-set object detector, to detect the bounding boxes of the target and surroundings. We then extract the segmentation masks of the entities using Mobile-SAM [56] and apply coordinate transformations to determine where the masks should be marked on the maps.

If the predicted progress value surpasses a threshold value, the agent will presumably have arrived at a location where the target is visible. As the final step, the agent has to determine the exact location of the target from the observations and move to a nearby position. The first method (MGP) is to select the bounding box with the largest confidence value in the target map and move to the center of the box. The second method (MGP + LLaVA) adopts the visual prompting method of Set-of-Mark prompting [53]. The RGB image is first annotated with labels based on the segmentation masks yielded by Semantic-SAM [26], and we prompt a vision language model LLaVA-1.6-34b [27] to select a label. The agent then moves to the center point of the bounding box corresponding to the segmentation mask of the selected label. In both of the two methods, the agent lowers its altitude to 5 meters above the ground level at the xy coordinates of the agent’s position.

2.4 Observation and Action Space

The observation space of Seq2Seq and CMA models consists of an RGB image, a depth image, and a description string. The resolution of the RGB and depth images are 224×224 and 256×256 respectively and the field of view of both images is 90 degrees. While MGP uses RGB and depth images with the same resolution for ResNet encoders, an RGB image with a resolution of 500×500 is used as the input for Grounding DINO and Mobile SAM.

The action space for all models consists of six actions: Stop, Move Forward, Move Up, Move Down, Turn Left, and Turn Right. The action Move Forward advances the agent 5 meters in the direction it is facing. Move Up and Move Down adjust the agent’s altitude by 2 meters, either raising or lowering it, respectively. Turn Left and Turn Right rotate the agent 30 degrees counterclockwise and clockwise, respectively.

2.5 Training

The CMA and Seq2Seq models were trained on a single NVIDIA H100 GPU and the MGP models were trained on a single GeForce RTX 4090 GPU. The hyperparameters used for training these models are given in Tab. 6 and 7.

To reduce the training and inference time we cached the target and surrounding maps. For each scene, we collected a set of phrases for unnamed entities from the descriptions using ChatGPT-3.5 Turbo. The scene was divided into a grid of squares with a side length of 100 m, and an image corresponding to an area of 40,000 m² was taken at each vertex of the grid. We then extracted the segmentation masks corresponding to each of the phrases for unnamed entities and aggregated the masks to form target/surrounding maps that covers the whole scene. The part of the maps corresponding to the view area of the agent was cropped to be used as the target/surrounding maps to speed up the training and inference process.

Table 6: Hyperparameters for training CMA and Seq2Seq

Hyperparameter	Value
Training Epochs	5
Optimizer	Adam [21]
Learning Rate	1.5e-3
Training Batch Size	12

Table 7: Hyperparameters for training MGP

Hyperparameter	Value
Training Epochs	10
Optimizer	AdamW [32]
Learning Rate	1.0e-3
Training Batch Size	8
Predicted Progress Threshold	0.75
Grounding DINO Bounding Box Threshold	0.15
Grounding DINO Text Threshold	0.25

3 Additional Quantitative Analysis

Tab. 8 and Tab. 9 show the navigation performance of the baseline models and the proposed model for the validation seen and validation unseen sets. The results follow the similar trend as the test unseen set in that the random and Seq2Seq agents are less successful on more difficult episodes and the MGP+LLaVA agent exhibits relatively consistent results across different difficulties.

4 Additional Qualitative Analysis

Figure 9 shows the additional qualitative results of our map-based goal predictor model. These examples also demonstrate the effectiveness of incorporating geographic information into the aerial model for locating target objects.

Table 8: Aerial navigation performance across difficulty levels (Val Seen)

Method	Easy				Medium				Hard			
	NE↓	SR↑	OSR↑	SPL↑	NE↓	SR↑	OSR↑	SPL↑	NE↓	SR↑	OSR↑	SPL↑
Random	130.4	0.00	3.41	0.00	211.7	0.00	0.00	0.00	323.7	0.00	0.00	0.00
Seq2Seq	270.3	2.92	14.01	2.35	265.0	1.15	4.20	1.11	236.6	1.33	5.33	1.26
CMA	253.7	0.73	14.49	0.71	233.2	1.02	10.45	1.00	235.1	1.09	3.39	1.06
MGP+LLaVA	64.7	8.73	49.40	7.96	55.7	9.67	40.15	9.26	58.7	7.72	17.54	7.66
Human	9.3	89.65	96.83	58.34	9.2	88.03	95.03	60.56	8.8	90.31	97.09	65.05

Table 9: Aerial navigation performance across difficulty levels (Val Unseen)

Method	Easy				Medium				Hard			
	NE↓	SR↑	OSR↑	SPL↑	NE↓	SR↑	OSR↑	SPL↑	NE↓	SR↑	OSR↑	SPL↑
Random	132.1	0.00	3.38	0.00	213.4	0.00	0.00	0.00	324.6	0.00	0.00	0.00
Seq2Seq	356.0	2.08	15.71	1.52	337.9	0.21	5.39	0.16	270.6	0.38	6.93	0.35
CMA	285.1	0.00	17.53	0.00	273.2	0.73	6.33	0.70	252.7	1.04	2.18	1.03
MGP+LLaVA	80.0	5.95	35.96	5.24	73.1	5.14	23.25	4.89	73.3	6.38	11.38	6.38
Human	10.1	86.36	95.71	56.16	9.5	88.38	95.64	64.35	9.0	89.85	95.16	67.42

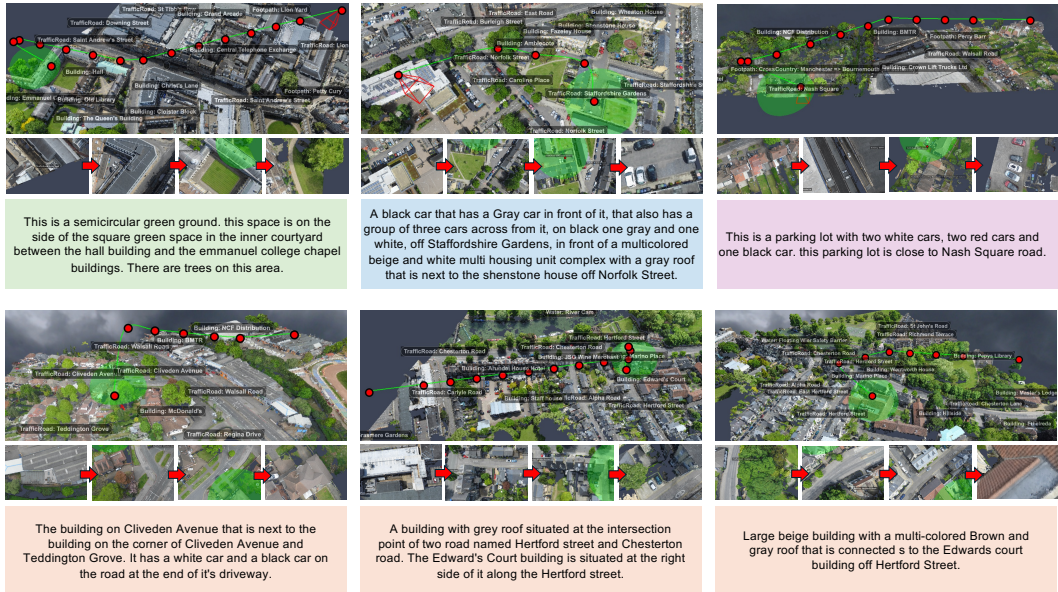


Figure 9: Additional qualitative examples of aerial navigation, illustrating the trajectories predicted by our map-based goal predictor model. The green upper hemisphere represents the area within a 20-meter radius around the target where navigation is successful.